

Geophysical Research Letters®



RESEARCH LETTER

10.1029/2022GL098566

Interpretable Deep Learning for Probabilistic MJO Prediction

Antoine Delaunay¹  and Hannah M. Christensen² 

¹Department of Applied Mathematics, Ecole Polytechnique, Palaiseau, France, ²Department of Physics, University of Oxford, Oxford, UK

Key Points:

- A deep convolutional neural network (CNN) is used to produce probabilistic forecasts of the Madden-Julian oscillation (MJO)
- The forecasts provide well-calibrated state-dependent estimates of forecast uncertainty
- The CNN forecasts are used to probe sources of predictability for the MJO

Supporting Information:

Supporting Information may be found in the online version of this article.

Correspondence to:

H. M. Christensen,
hannah.christensen@physics.ox.ac.uk

Citation:

Delaunay, A., & Christensen, H. M. (2022). Interpretable deep learning for probabilistic MJO prediction. *Geophysical Research Letters*, 49, e2022GL098566. <https://doi.org/10.1029/2022GL098566>

Received 14 MAR 2022

Accepted 20 AUG 2022

Author Contributions:

Conceptualization: Hannah M. Christensen
Formal analysis: Antoine Delaunay
Investigation: Antoine Delaunay
Methodology: Antoine Delaunay, Hannah M. Christensen
Software: Antoine Delaunay
Supervision: Hannah M. Christensen
Validation: Antoine Delaunay
Visualization: Antoine Delaunay
Writing – original draft: Antoine Delaunay, Hannah M. Christensen
Writing – review & editing: Antoine Delaunay, Hannah M. Christensen

Abstract The Madden-Julian oscillation (MJO) is the dominant source of sub-seasonal variability in the tropics. It consists of an Eastward moving region of enhanced convection coupled to changes in zonal winds. It is not possible to predict the precise evolution of the MJO, so sub-seasonal forecasts are generally probabilistic. We present a deep convolutional neural network (CNN) that produces skilful state-dependent probabilistic MJO forecasts. Importantly, the CNN's forecast uncertainty varies depending on the instantaneous predictability of the MJO. The CNN accounts for intrinsic chaotic uncertainty by predicting the standard deviation about the mean, and model uncertainty using Monte-Carlo dropout. Interpretation of the CNN mean forecasts highlights known MJO mechanisms, providing confidence in the model. Interpretation of forecast uncertainty indicates mechanisms governing MJO predictability. In particular, we find an initially stronger MJO signal is associated with more uncertainty, and that MJO predictability is affected by the state of the Walker Circulation.

Plain Language Summary The Madden-Julian oscillation (MJO) is an important tropical climate phenomenon. It consists of enhanced convective thunderstorms and anomalous winds that propagate eastward along the Equator for a few weeks. The MJO is difficult to predict and exhibits great variability. This means that forecasts are often probabilistic. However, current models have difficulty in correctly predicting the uncertainty in the forecast based on the current conditions. In this paper, we propose a model using neural networks capable of making reliable probabilistic forecasts. We interpret the behavior of the algorithm to verify its consistency with the known physical mechanisms of the MJO and to highlight new physical conditions that affect MJO prediction uncertainty.

1. Introduction

The Madden-Julian oscillation (MJO; Madden & Julian, 1971) is an envelope of enhanced tropical convection with associated changes to the atmospheric circulation. It is characterized by its period of 40–50 days, its planetary scale, and its Eastward propagation at speeds of 4–8 ms⁻¹. It is the major source of predictability on sub-seasonal timescales in the Tropics (Zhang, 2013) and influences phenomena such as the North Atlantic Oscillation and Arctic sea ice cover through global teleconnections (Cassou, 2008; Ferranti et al., 1990; Henderson et al., 2014; Yoo et al., 2012). Subseasonal forecasts are of great socio-economic value through their potential to predict extreme weather events several weeks ahead (Vitart & Robertson, 2018). There is therefore great interest in improving predictions of the MJO, and in understanding sources of MJO predictability (Kim et al., 2018).

The chaotic nature of the Earth System means that it is not possible to predict the precise evolution of the MJO beyond a few days, so subseasonal forecasts are generally probabilistic (Bauer et al., 2015; J. Slingo & Palmer, 2011). If the probabilistic forecast *mean* is assessed, averaging out the unpredictable “noise,” current dynamical models have a prediction skill up to 3 weeks (Lim et al., 2018; Vitart, 2017). However, systematic biases remain, especially in the propagation of the MJO convective anomaly over the Maritime Continent (Barrett et al., 2021; Kim et al., 2016; Li et al., 2020). In contrast to the mean skill, the *probabilistic* skill of MJO forecasts is low (Lim et al., 2018; Vitart, 2017). Improving probabilistic forecasts is essential to quantify our confidence in the predictions, and to advance understanding of the predictability of this phenomenon.

While prediction skill is a property of the forecast model, predictability is a property of the Earth-system. MJO predictability studies have focused on the theoretically achievable prediction limit that one could achieve with a perfect model, quantified as 6–7 weeks (e.g., Kim et al., 2018; Neena et al., 2014; Wu et al., 2016). This is complementary to an approach taken in the medium-range forecasting community, where “predictable” forecasts are those for which the forecast uncertainty is small (e.g., Palmer, 2000). This identification is possible because medium-range forecasts exhibit state-dependent reliability (Leutbecher & Palmer, 2008). If reliable,

© 2022. The Authors.

This is an open access article under the terms of the [Creative Commons Attribution License](https://creativecommons.org/licenses/by/4.0/), which permits use, distribution and reproduction in any medium, provided the original work is properly cited.

state-dependent, MJO forecasts could be produced, forecast uncertainty could be used as an indicator of instantaneous MJO predictability.

Increasing volumes of data, advances in computational power, and developments in statistical modeling have led to substantial interest in the use of machine learning in Earth-system science (Huntingford et al., 2019; Reichstein et al., 2019). Deep learning has been applied to the MJO for phase classification (Martin et al., 2021; Toms et al., 2020), post processing (Kim et al., 2021), and deterministic prediction (Martin et al., 2021). Here, we develop a neural network that produces well calibrated probabilistic forecasts of the MJO. We use a convolutional neural network (CNN), which has proved effective at identifying hidden patterns and processes in climate (Arcomano et al., 2020; Ham et al., 2019; Schultz et al., 2021) and other areas such as image recognition (Russakovsky et al., 2015).

The paper is structured as follows: in Section 2, we describe the CNN, including the data used to train the model. In Section 3 we present our results. We evaluate the CNN compared to dynamical models from the subseasonal-to-seasonal (S2S) prediction project. We validate the CNN by seeking to understand its mean forecasts, before using the CNN to uncover potential sources of predictability for the MJO. Finally we discuss the significance of our results and draw conclusions in Section 4.

2. Methods

2.1. Data

Observational data used to train and test the CNN are taken from the ECMWF Reanalysis version 5 (ERA5) data set between 1979 and 2019 (Hersbach, et al., 2020). We compare the CNN to models from the S2S database (F. Vitart et al., 2017). We select reforecast data from four representative models, chosen to span the range of performances of models in the S2S database. In particular, we include the European Centre for Medium-Range Weather Forecasts (ECMWF) model, which is known to produce the most skilful MJO forecasts (Lim et al., 2018). The remaining models chosen had the largest reforecast ensemble size, enabling probabilistic forecast skill to be assessed. Details are presented in Table S1 and Text S1 of Supporting Information S1.

2.2. Overview of Predictive Model

The MJO is a coupled convective-dynamic anomaly that can be summarized by the bivariate real-time multivariate MJO (RMM) index (Wheeler & Hendon, 2004). The RMM index classifies active MJO events (amplitude greater than one) into one of eight phases depending on geographical location (e.g., Figure S1 in Supporting Information S1). Using observed daily-mean maps for a single date t as inputs, we train a deep CNN to predict the mean and uncertainty in RMM1 and RMM2 computed from daily means at a later date $t + \tau$, training a separate CNN for each lead time. The chosen lead times are one, three and 5 days, then every fifth day up to 35 days. The architecture of the CNN is shown in Figure S2 of Supporting Information S1.

We compute the observed values of the RMM following Wheeler and Hendon (2004) (Text S2 in Supporting Information S1). Subseasonal anomalies of daily-mean outgoing longwave radiation (OLR) and daily-mean zonal winds at 200 hPa (UA200) and 850 hPa (UA850) between 20°S and 20°N are latitudinally averaged and divided by their global variance. The first two empirical orthogonal functions (EOFs) of the combined fields are computed. RMM1 and RMM2 are the projection of the daily fields onto EOFs 1 and 2.

Even though the MJO shows seasonal behavior, we train a single model for all seasons to maximize the available training data. As inputs we use subseasonal anomalies of OLR, UA200, and UA850, consistent with fields used to compute the RMM indices. We supplement these with four further fields which provide complementary information: daily mean Specific Humidity at 400 hPa (SHUM400) was included because Barrett et al. (2021) reported large differences in SHUM400 between MJO events which propagate and weaken over the Maritime Continent; daily mean geopotential at 850 hPa (Z850) provided skill in previous work (Toms et al., 2020); daily mean downwelling longwave radiation at the surface has a marked annual cycle, which we found a more effective means of accounting for the seasonality of the MJO than including a dummy variable. Finally, daily anomalies of sea surface temperature (SST) are included, since the MJO is known to be linked to El Niño-Southern Oscillation (ENSO; e.g., Kessler, 2001). Sensitivity of CNN performance to the choice of input feature is shown in Figure S3 of Supporting Information S1, providing insights into sources of predictability for the MJO. Inputs are provided

as maps spanning 0–360°E, 20°S–20°N on a $2.5^\circ \times 2.5^\circ$ grid. The different variables are input to the CNN as separate channels. This allows the CNN to learn to identify co-located phenomena. To ensure independence between the training and testing data sets, we use the first 80% of the dates for training, and the remaining 20% for testing.

We model the two forecast RMM indices as following a Gaussian Bivariate distribution with null correlation (Wheeler & Hendon, 2004). The network outputs the predicted means and variances of RMM1 and RMM2, and is trained by minimizing the negative log-likelihood. The output variance represents the intrinsic chaotic (aleatoric) uncertainty in the prediction. In addition, we represent the epistemic uncertainty in the CNN model weights using a Monte-Carlo Dropout method to produce an ensemble of forecasts (Gal, 2016; Gal & Ghahramani, 2016; Scalia et al., 2019). The total forecast uncertainty is the sum of the aleatoric and epistemic variances. More details are provided in Text S3 of Supporting Information S1.

2.3. Interpretation Using PatternNet

We use the PatternNet algorithm (Kindermans et al., 2017) to interpret forecasts made by the CNN, as it outperforms other approaches including Guided BackProp and Layerwise Relevance Propagation in both idealized test cases and for image classification problems (Kindermans et al., 2017). Inputs to the CNN include a *signal*, that contains information about the future state of the MJO, and a *distractor*, that is a residual containing information irrelevant to the prediction task (Kindermans et al., 2017). PatternNet is a distinct network to the CNN, but whose structure reflects that of the CNN in reverse, propagating the estimated signal from the output to the input space, thereby disentangling the signal from the distractor: for more details, see Text S4 in Supporting Information S1.

3. Results

3.1. Network Performance

Figure 1 compares the network's performance to models from the S2S database (see Text S5 in Supporting Information S1 for definitions of all metrics). Figures 1a–1c show the deterministic skill of the CNN mean forecasts in terms of the root mean square error (RMSE), Amplitude Error, and Phase Error respectively. In terms of RMSE, the CNN is competitive with models from the S2S database, though has larger errors than ECMWF. Similarly to the dynamical models, the CNN forecasts suffer from an increasing amplitude error with time, indicating a decay in MJO strength over the duration of the forecast. It is known that dynamical models simulate slower MJO propagation speeds than observed, resulting in a negative phase error (Lim et al., 2018). Here the CNN outperforms the dynamical models, accurately capturing the MJO propagation speed. A fourth metric, the bivariate correlation, is shown in Figure S4 of Supporting Information S1: the CNN performance is poorer than ECMWF, but similar to CNRM and BOM.

Figures 1d–1f assess the probabilistic skill of the CNN. The continuous ranked probability score (CRPS: Marshall et al. (2016)) compares forecast and observed cumulative distribution functions. The CNN is competitive with forecasts from the S2S database, outperforming three of the four dynamical models considered. Despite being widely used, the CRPS can give unintuitive rankings (e.g., Bolin & Wallin, 2019), as it penalizes errors in the forecast mean more than poor calibration of spread (Christensen et al., 2015). An alternative score is the “Ignorance” or log-score (Roulston & Smith, 2002) (Panel e). This score is local, derived from information theory, and easily generalizes to multivariate predictions (Bjerregård et al., 2021; Roulston & Smith, 2002). It is also consistent with the loss function used to train the network. According to the log-score, the CNN is one of the two models with the best forecast skill at lead times of 5–35 days. At shorter lead times, it outperforms all dynamical models. The poor performance of dynamical models at these short lead times is due to overconfident forecasts (Bjerregård et al., 2021), which are penalized by the log-score. In contrast, the CNN is able to balance the loss in accuracy with an increasing predicted uncertainty as the lead time increases.

For probabilistic forecasts to be useful, observations should behave as if they were drawn from the forecast probability distribution. For this to hold, a smaller forecast spread should indicate a smaller root mean squared error (RMSE) in the forecast mean on average. We assess this property using Error-Spread diagrams (Leutbecher & Palmer, 2008) shown in Figure 2. The RMSE is a measure of predictability of the atmosphere: high RMSE indicates lower predictability. The spread indicates the forecast model's belief about the predictability. For well

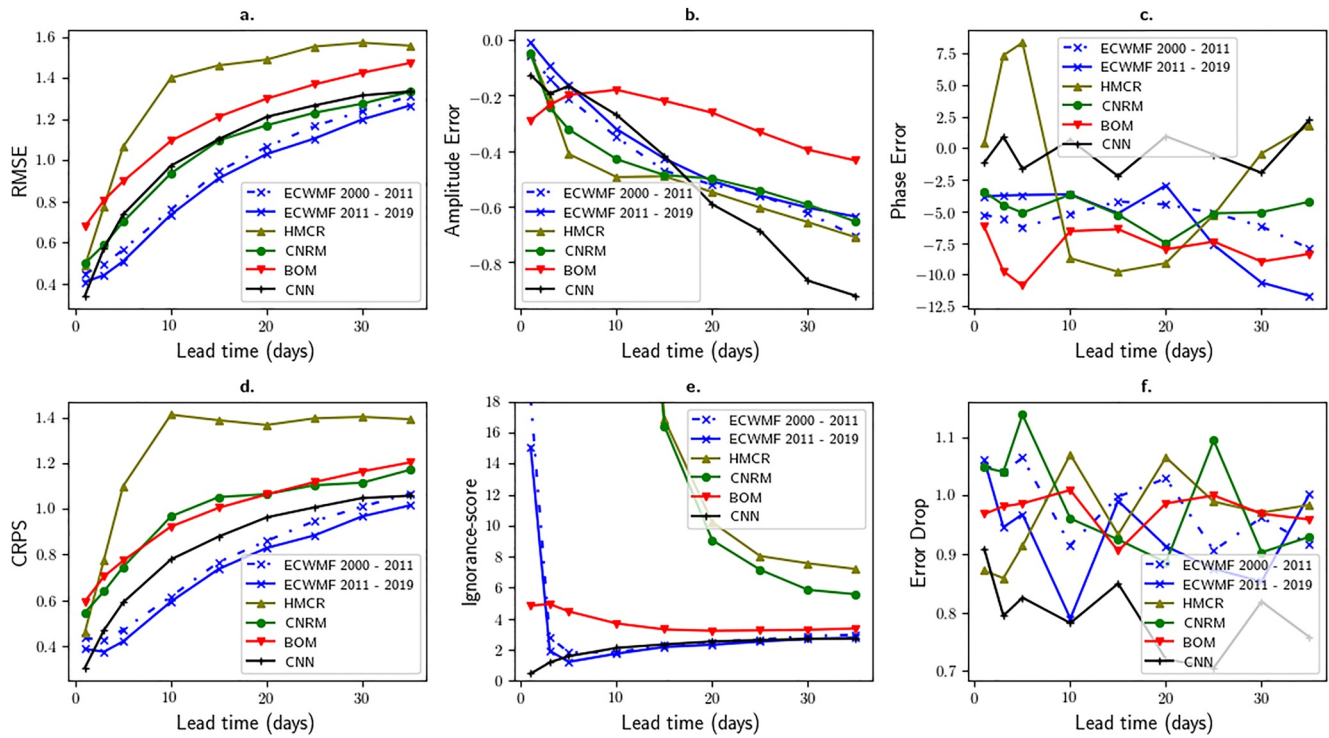


Figure 1. Skill of convolutional neural network (CNN) (black), compared to forecasts from the subseasonal-to-seasonal prediction project (colors) as a function of lead time. (a) Root mean square error. (b) Amplitude error. (c) Phase error. (d) Continuous ranked probability score. (e) Log-score. CNRM and HMCR scores before day-15 were too high to be shown. (f) Error-Drop. For all scores, a value closer to zero indicates a more skilful forecast. Forecasts from different models cover: European Center for Medium-Range Weather Forecasts (ECMWF) 2000–2019; Hydrometeorological Centre of Russia (HMCR) 1985–2010; Météo-France/Centre National de Recherche Meteorologiques (CNRM) 1993–2017; Australian Bureau of Meteorology (BOM) 1982–2013; CNN 2011–2019. The ECMWF data was split into two to allow direct comparison with the CNN over 2011–2019, and to give an indication of sampling uncertainty.

calibrated forecasts, RMSE and spread should be correlated, and the observed RMSE should equal the predicted standard deviation, with scattered points lying on the one-to-one line. None of the dynamical models have this property: their error distributions are independent of the forecast spread, such that the spread gives no indication of the true predictability of the MJO on that day. In contrast, if the CNN forecast spread is low, the RMSE is

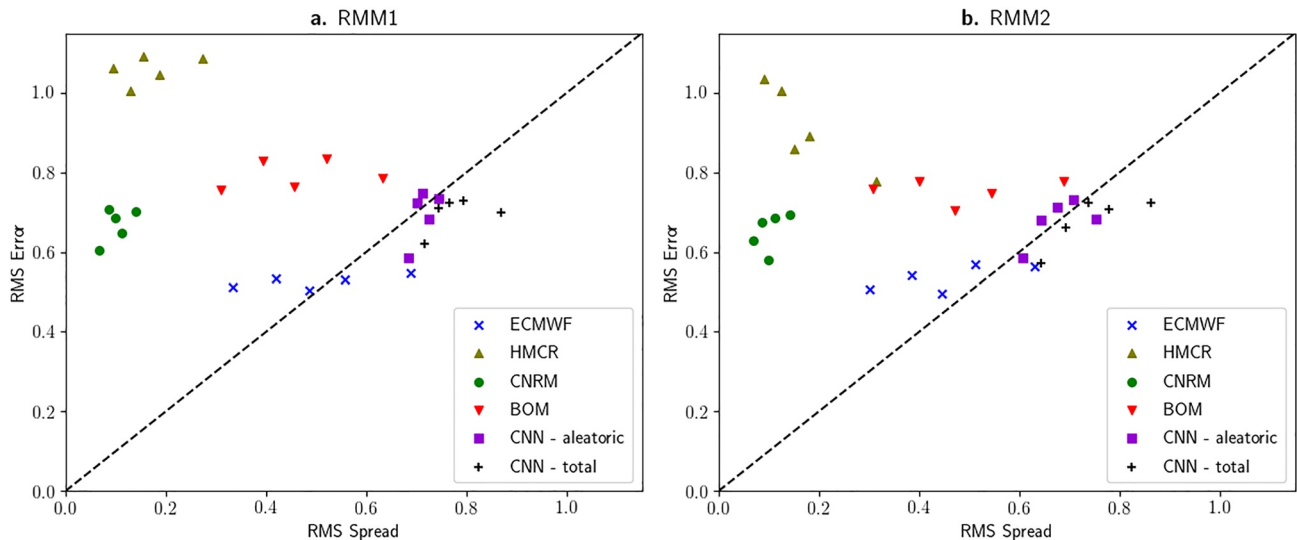


Figure 2. Error-spread diagrams for (a) RMM1 and (b) RMM2 at a lead time of 10 days. The data are sorted according to the predicted spread before being split into five quintiles. The figure shows the average spread and RMSE for each quintile. Well calibrated forecasts lie on the one-to-one dashed line.

smaller than if the spread is high. The probabilistic forecasts produced by the CNN are a dynamic indicator of the certainty in the MJO forecasts, and therefore the instantaneous predictability of the MJO. The aleatoric uncertainty predicted by the CNN is substantially greater than the epistemic uncertainty, indicating that while the MJO exhibits chaotic unpredictability, the CNN weights are well constrained by the available data.

To quantify this property across many lead times, we incrementally remove the days with the highest predicted variance for each lead time and RMM index before computing the RMSE in the forecast of the remaining days. This produces the confidence curve (Scalia et al., 2019). If the forecast correctly ranks different days in terms of forecast uncertainty, the confidence curve should be strictly decreasing. The error-drop (Figure 1f), is the ratio between the last and first points on the confidence curve (Scalia et al., 2019). The smaller the error-drop, the greater the reduction in RMSE when test days are sorted by the forecast uncertainty. The CNN performs better than all dynamical models. It can distinguish between predictable and unpredictable days at all lead times. While an under-dispersive ensemble spread can be corrected to improve the log-score of dynamical models (Figure 1), the ability to sort days according to their predictability cannot be introduced by statistical post-processing.

3.2. Interpretation to Validate Network Behavior

Before using the CNN to understand sources of uncertainty in the evolution of the MJO, we must understand how the CNN can make skilful forecasts of the MJO. This is necessary, as it reveals any concerning behavior or spurious correlations (e.g., Lapuschkin et al., 2019), lending confidence to the predictions.

To interpret the CNN mean forecasts, we use the PatternNet algorithm (Kindermans et al., 2017) to derive signal maps for each forecast. These indicate where information is detected by the CNN in each input field. Because the different input variables are introduced as separate channels into the CNN, weights are shared across all variables for much of the network: the CNN distinguishes between variables in the first layer only. It is therefore useful to consider both the signal maps averaged over all variables (the *signal mean*) and the difference between the signal map for each variable and the signal mean map (the *signal anomalies*).

Since propagation over the Maritime Continent is a source of error in MJO forecasts in many models (Kim et al., 2016), we contrast one event which propagated over the Maritime Continent (28 February 2012), and one which decayed (25 February 2006) to validate the CNN's behavior. Figure S1 in Supporting Information S1 shows the observed RMM indices for these two events, and the corresponding mean forecasts initialized in phase 3, which capture the observed behavior.

Figures 3a and 3b show the SHUM400 input fields averaged over all days in RMM phase 3 for the decaying and the propagating events respectively. Panels (c and d) show the signal means for RMM1 for the associated 10-day CNN forecasts initialized in phase 3. (The signal means for the decaying RMM2 are much smaller, consistent with the prediction that day-10 RMM2 is close to zero for the events selected: see Figure S5 in Supporting Information S1). For both events, the CNN signal mean maps show that the CNN integrates over a large region spanning the Indian and Pacific Oceans, rather than tightly focusing on the active MJO region: the CNN also derives information from the input fields in regions of suppressed convection (Barrett et al., 2021; Feng et al., 2015).

Figures 3e and 3f show the corresponding PatternNet signal anomalies for SHUM400, highlighting the relative information provided by this input field. We see a large reduction in signal over the Pacific (150°E–90°W), and an enhancement over the Maritime Continent (90°–110°E) co-located with enhanced SHUM400. Figures S6–S7 in Supporting Information S1 show the equivalent figure for OLR. The RMM1 signal anomaly is greater than for SHUM400, and it is stronger over the Pacific than was the case for SHUM400. Both Feng et al. (2015) and Barrett et al. (2021) found OLR precursors in this region which distinguished between propagating and non-propagating MJO events. We conclude that the CNN has identified true predictive features of MJO propagation, giving us confidence in the network.

3.3. Predictors of Uncertainty in MJO Forecasts

The ability of the CNN to rank days by uncertainty enables us to investigate drivers of short-term predictability of the MJO. We consider cases in Boreal winter, and separate MJO events into four categories according to the CNN's 10-day forecast. We first categorize according to strength: for each day, an event is weak (strong) if the

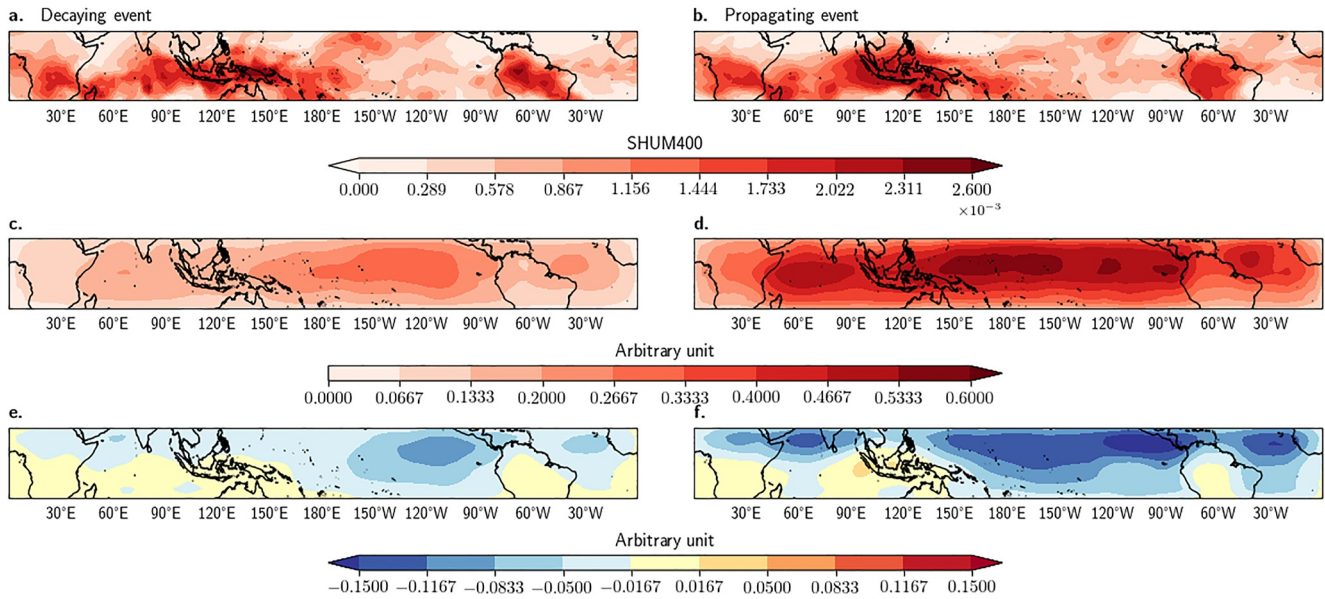


Figure 3. Interpretation of convolutional neural network (CNN) mean forecasts. (a, b) Composite maps of phase-3 Specific Humidity at 400 hPa (SHUM400) for a Madden-Julian oscillation event which (a) decays and (b) propagates over the Maritime Continent. (c, d) PatternNet RMM1 signal means (averaged over all variables) for 10-day forecasts for the decaying and propagating event respectively. (e, f) RMM1 signal anomalies in SHUM400 for the decaying and propagating events respectively.

initial observed RMM amplitude is less than (greater than) 1.0. The data are then divided into certain and uncertain forecasts. To study the uncertainty that is directly linked to the MJO initial conditions, we use the network's predicted aleatoric uncertainty. An event is certain (uncertain) if both the RMM1 and RMM2 forecast aleatoric uncertainties are under (over) their respective 30% (70%) percentiles. For each initial observed phase and input feature, we compute the difference between certain and uncertain days, separately for weak and strong events.

Figure 4 shows results for SHUM400 for events starting in phases 3 and 7. For phase 3, the initial conditions of “certain” forecasts have reduced humidity at the equator in the central Pacific (150°E–120°W) and Indian Ocean (45°–100°E), combined with off-equatorial regions of enhanced humidity over the Maritime Continent

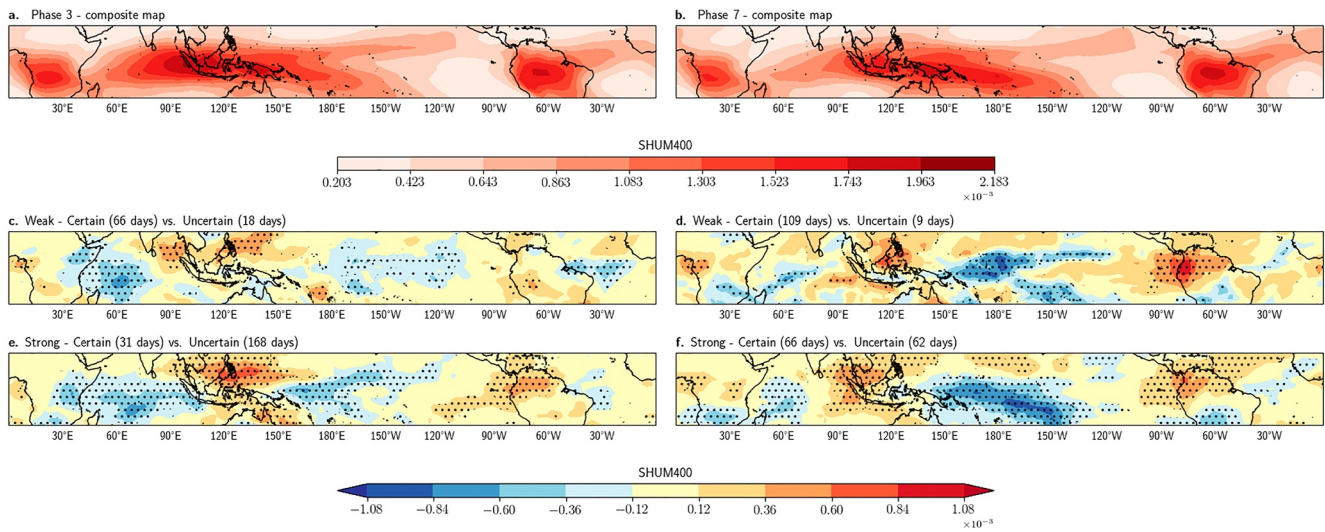


Figure 4. Interpretation of convolutional neural network (CNN) uncertainty forecasts. (a, b) Composite maps of specific Humidity at 400 hPa (SHUM400) for extended Boreal winter Madden-Julian oscillation events in (a) phase 3 and (b) phase 7. (c–f) Difference between input maps for predictable and unpredictable events as classified by 10-day forecasts using the CNN. (c) Weak phase 3 events (d) weak phase 7 events. (e) Strong phase 3 events (f) strong phase 7 events. Stippling denotes areas where anomalies are significant at the 95% level using the Student's *t*-test.

and Australia (100° – 160° E). Before concluding that this “fingerprint” is an indicator of high certainty, there are two possible confounding factors to consider: the initial strength of the signal, and the forecast strength at day-10. The difference maps for weak and strong events are similar to each other, indicating the fingerprint is independent of initial strength. However, there is a correlation between the forecast uncertainty and the forecast strength at day-10: $\sim 65\%$ of “certain” events are forecast as weak by day-10, while $\sim 80\%$ of “uncertain” events are forecast strong at day-10 (Table S3 in Supporting Information S1). Therefore sorting the data by forecast certainty unintentionally also sorts by forecast strength. To remove this confounding factor, we further stratified the events by strength at day-10. The moisture signal was muted if all events forecast as weak at day-10 were removed from the composites, whereas if only events forecast as transitioning from strong to weak were considered, the signal became more intense (not shown). This confirms that the fingerprint is primarily an indicator of forecast strength at day-10, consistent with the conclusions of Jiang et al. (2020) who found that this structure hinders the eastward propagation of the MJO.

For events initialized in phase 7, uncertain events show reduced moisture over the Maritime Continent in the MJO suppressed region (90° – 120° E), and enhanced moisture over the MJO active region (150° E– 150° W), when compared to certain events. This signature of an enhanced MJO signal in the initial conditions for unpredictable events is observed for other variables for phase 7, particularly OLR (Figure S8 in Supporting Information S1). For events initialized in phase 7, 85% of uncertain forecasts are also likely to be strong at day-10, whereas that drops to 40% for certain forecasts (Table S4 in Supporting Information S1). However, if we further stratify the forecasts by final strength, we find the signature persists (not shown). Thus we conclude that an initially stronger MJO signal is associated with more uncertainty in the forecast.

Finally, we find that MJO predictability is affected by the background state through which it propagates. In particular, for events classified as certain, Z850 shows an enhanced gradient between the Eastern Pacific and the Maritime Continent for all forecasts initialized in phases 4–7 (i.e., all events crossing the Pacific: Figure S9–S10 in Supporting Information S1). An enhanced Z850 gradient is consistent with a higher Southern Oscillation index and a stronger Walker circulation cell over the Pacific. Further stratification by strength at day-10 indicates that this signal is unrelated to forecast strength. An enhanced (neutral or weakened) Walker circulation therefore leads to enhanced (reduced) certainty in the MJO.

4. Discussion and Conclusions

We presented a CNN which produces probabilistic forecasts of the MJO in terms of means and variances of the bivariate RMM index. The skill of the CNN is competitive with models from the S2S database. Moreover, the CNN outperforms all S2S models for one key forecast property: it can rank start dates according to the forecast uncertainty associated with the initial conditions. In other words, the CNN forecast spread is a dynamic indicator of the uncertainty in the MJO forecast on a given day.

Since the CNN exhibits state-dependent reliability, we identify “certain” CNN forecasts with predictable states of the MJO and use the CNN forecasts to probe associated sources of predictability. We do this by considering composites of initial conditions which the CNN indicated led to “certain” and “uncertain” 10-day forecasts. We found that for forecasts initialized in phase 3, reduced humidity on the equator increases the likelihood of a decaying MJO event, which is associated with high forecast certainty. However, enhanced humidity on the equator increases the likelihood of MJO propagation over the MC, but it does not guarantee propagation, leading to high uncertainty in the forecast and low medium-range predictability.

The CNN also used background state information to determine the MJO's instantaneous predictability. A reduced gradient in Z850 was linked to more forecast uncertainty for all MJO phases approaching the Pacific. This change in Z850 reflects a weaker Walker circulation, associated with El-Niño events. However, we found no consistent signal in East Pacific SST across these phases (Figures S11–S12 in Supporting Information S1). There is substantial debate about the dependency of the MJO on the state of the El Niño-Southern Oscillation (ENSO) (e.g., Ling et al., 2017). The Eastward extent of MJO activity is greater in El Niño years, (Kessler, 2001), and the MJO lifetime and propagation speed is also modulated by ENSO, though it shows sensitivity to the season of interest and type of ENSO event (Pang et al., 2016; Pohl & Matthew, 2007). In contrast, the overall amplitude of MJO activity appears unrelated to ENSO (Kessler, 2001; J. M. Slingo et al., 1999). While the dependency of the MJO

on the back-ground state is usually considered in terms of SST, our results demonstrate ENSO could primarily influence the MJO via changes to the atmospheric dynamical background associated with El Niño and La Niña.

Our CNN approach is complementary to earlier MJO predictability studies (e.g., Kim et al., 2018; Neena et al., 2014; Wu et al., 2016). Instead of quantifying the potential predictability *limit* using our model, we assess relative predictability in the medium-range across different initial conditions. We can only do this because the CNN produces state dependent reliable probabilistic forecasts. Our focus was on forecasts at a lead time of 10-days. Longer lead time forecasts may show a different signal of predictability in the initial conditions: for example, while we found that a weak MJO event predictably decays over a 10-day period, the situation after those 10-days is likely to be more unpredictable than for events where the MJO persists beyond the 10-day period.

The CNN is competitive with the best available dynamical models at predicting the MJO. However CNNs are complementary to dynamical models, and further improvements to MJO forecasting may be achieved through a blend of dynamical and machine learning approaches (Kim et al., 2021). Nevertheless, developing a stand-alone CNN facilitates interpretation, enabling us to probe the performance of the CNN and develop new physical understanding, for example, the role of different input features. This framework of combining state-dependent uncertainty estimates from neural networks with interpretation techniques could be applied to other climate phenomena, allowing us to quantify the diverse range of sources of uncertainty in the Earth System.

Data Availability Statement

Data related to this paper can be downloaded from the ERA5 Copernicus database (<https://cds.climate.copernicus.eu/cdsapp#!/dataset/reanalysis-era5-pressure-levels>, <https://cds.climate.copernicus.eu/cdsapp#!/dataset/reanalysis-era5-single-levels>) and the S2S project archive (<http://s2sprediction.net>) via the European Centre for Medium-Range Weather Forecasts portal (<https://apps.ecmwf.int/datasets/data/s2s-reforecasts-instantaneous-accum-ecmf/>; <https://apps.ecmwf.int/datasets/data/s2s-reforecasts-instantaneous-accum-rums/>; <https://apps.ecmwf.int/datasets/data/s2s-reforecasts-instantaneous-accum-lfpw/>; <https://apps.ecmwf.int/datasets/data/s2s-reforecasts-instantaneous-accum-ammc/>). The convolutional neural network (CNN) forecasts produced for this paper can be downloaded from <https://doi.org/10.5281/zenodo.5175837>. The RMM indices were computed using the CLIVAR diagnostics package (<https://www.ncl.ucar.edu/Applications/mjoclivar.shtml>). PyTorch (<https://pytorch.org>) and DropBlock (<https://github.com/miguelvr/dropblock>) libraries were implemented to build and train the CNN model. PatternNet code was adapted from https://github.com/TNTLFreiburg/pytorch_patternnet. The codes used in the current analysis are available at <https://github.com/antoine-de-launay/DeepLearningMJO/>.

Acknowledgments

H.M.C. was funded by Natural Environment Research Council grant number NE/P018238/1. Thanks to D.J. Gagne and an anonymous reviewer for their comments which improved this manuscript.

References

- Arcomano, T., Szunyogh, I., Pathak, J., Wikner, A., Hunt, B. R., & Ott, E. (2020). A machine learning-based global atmospheric forecast model. *Geophysical Research Letters*, 47(9), e2020GL087776. <https://doi.org/10.1029/2020gl087776>
- Barrett, B. S., Densmore, C. R., Ray, P., & Sanabia, E. R. (2021). Active and weakening MJO events in the Maritime Continent. *Climate Dynamics*, 57(1–2), 157–172. <https://doi.org/10.1007/s00382-021-05699-8>
- Bauer, P., Thorpe, A., & Brunet, G. (2015). The quiet revolution of numerical weather prediction. *Nature*, 525(7567), 47–55. Retrieved from <http://www.nature.com/doi/10.1038/nature14956>
- Bjerrgård, M. B., Møller, J. K., & Madsen, H. (2021). An introduction to multivariate probabilistic forecast evaluation. *Energy and AI*, 4, 100058. <https://doi.org/10.1016/j.egyai.2021.100058>
- Bolin, D., & Wallin, J. (2019). Local scale invariance and robustness of proper scoring rules (Vol. 1–26). Retrieved from <http://arxiv.org/abs/1912.05642>
- Cassou, C. (2008). Intraseasonal interaction between the Madden-Julian oscillation and the North Atlantic oscillation. *Nature*, 455(7212), 523–527. <https://doi.org/10.1038/nature07286>
- Christensen, H. M., Moroz, I. M., & Palmer, T. N. (2015). Evaluation of ensemble forecast uncertainty using a new proper score: Application to medium-range and seasonal forecasts. *Quarterly Journal of the Royal Meteorological Society*, 141(687), 538–549. <https://doi.org/10.1002/qj.2375>
- Feng, J., Li, T., & Zhu, W. (2015). Propagating and nonpropagating MJO events over Maritime Continent. *Journal of Climate*, 28(21), 8430–8449. <https://doi.org/10.1175/JCLI-D-15-0085.1>
- Ferranti, L., Palmer, T., Molteni, F., & Klinker, E. (1990). Tropical-extratropical interaction associated with the 30–60 day oscillation and its impact on medium and extended range prediction. *Journal of the Atmospheric Sciences*, 47(18), 2177–2199. [https://doi.org/10.1175/1520-0469\(1990\)047<2177:teiawt>2.0.co;2](https://doi.org/10.1175/1520-0469(1990)047<2177:teiawt>2.0.co;2)
- Gal, Y. (2016). *Uncertainty in deep learning (Unpublished doctoral dissertation)*. Cambridge University.
- Gal, Y., & Ghahramani, Z. (2016). Dropout as a Bayesian approximation: Representing model uncertainty in deep learning. In *International conference on machine learning* (pp. 1050–1059).
- Ham, Y.-G., Kim, J.-H., & Luo, J.-J. (2019). Deep learning for multi-year ENSO forecasts. *Nature*, 573(7775), 568–572. <https://doi.org/10.1038/s41586-019-1559-7>

- Henderson, G. R., Barrett, B. S., & Lafleur, D. (2014). Arctic sea ice and the Madden-Julian oscillation (MJO). *Climate Dynamics*, 43(7–8), 2185–2196. <https://doi.org/10.1007/s00382-013-2043-y>
- Hersbach, H., Bell, B., Berrisford, P., Hirahara, S., Horanyi, A., Munoz-Sabater, J., et al. (2020). The ERA5 global reanalysis. *Quarterly Journal of the Royal Meteorological Society*, 146(730), 1999–2049. <https://doi.org/10.1002/qj.3803>
- Huntingford, C., Jeffers, E. S., Bonsall, M. B., Christensen, H. M., Lees, T., & Yang, H. (2019). Machine learning and artificial intelligence to aid climate change research and preparedness. *Environmental Research Letters*, 14(12), 124007. <https://doi.org/10.1088/1748-9326/ab4e55>
- Jiang, X., Maloney, E., & Su, H. (2020). Large-scale controls of propagation of the Madden-Julian oscillation. *Npj Climate and Atmospheric Science*, 3(1), 29. <https://doi.org/10.1038/s41612-020-00134-x>
- Kessler, W. S. (2001). EOF representations of the Madden-Julian and its connection with ENSO. *Journal of Climate*, 14(13), 3055–3061. [https://doi.org/10.1175/1520-0442\(2001\)014<3055:erotmj>2.0.co;2](https://doi.org/10.1175/1520-0442(2001)014<3055:erotmj>2.0.co;2)
- Kim, H., Ham, Y. G., Joo, Y. S., & Son, S. W. (2021). Deep learning for bias correction of MJO prediction. *Nature Communications*, 12(1), 3087. <https://doi.org/10.1038/s41467-021-23406-3>
- Kim, H., Kim, D., Vitart, F., Toma, V. E., Kug, J.-S., & Webster, P. J. (2016). MJO propagation across the Maritime Continent in the ECMWF ensemble prediction system. *Journal of Climate*, 29(11), 3973–3988. <https://doi.org/10.1175/jcli-d-15-0862.1>
- Kim, H., Vitart, F., & Waliser, D. E. (2018). Prediction of the Madden-Julian oscillation: A review. *Journal of Climate*, 31(23), 9425–9443. <https://doi.org/10.1175/JCLI-D-18-0210.1>
- Kindermans, P.-J., Schütt, K. T., Alber, M., Müller, K.-R., Erhan, D., Kim, B., & Dähne, S. (2017). Learning how to explain neural networks: PatternNet and PatternAttribution. Retrieved from <http://arxiv.org/abs/1705.05598>
- Lapuschkin, S., Wäldchen, S., Binder, A., Montavon, G., Samek, W., & Müller, K. R. (2019). Unmasking Clever Hans predictors and assessing what machines really learn. *Nature Communications*, 10(1), 1–8. <https://doi.org/10.1038/s41467-019-08987-4>
- Leutbecher, M., & Palmer, T. (2008). Ensemble forecasting. *Journal of Computational Physics*, 227(7), 3515–3539. <https://doi.org/10.1016/j.jcp.2007.02.014>
- Li, X., Yin, M., Chen, X., Yang, M., Xia, F., Li, L., et al. (2020). Impacts of the tropical Pacific–Indian Ocean associated mode on Madden-Julian oscillation over the Maritime Continent in boreal winter (Vol. 14).
- Lim, Y., Son, S.-W., & Kim, D. (2018). MJO prediction skill of the subseasonal-to-seasonal prediction models. *Journal of Climate*, 31(10), 4075–4094. <https://doi.org/10.1175/JCLI-D-17-0545.1>
- Ling, J., Li, C., Li, T., Jia, X., Khouider, B., Maloney, E., et al. (2017). Challenges and opportunities in MJO studies. *Bulletin of the American Meteorological Society*, 98(2), ES53–ES56. <https://doi.org/10.1175/BAMS-D-16-0283.1>
- Madden, R. A., & Julian, P. R. (1971). Detection of a 40–50 day oscillation in the zonal wind in the Tropical Pacific. *Journal of the Atmospheric Sciences*, 28(5), 702–708. <https://doi.org/10.1017/CBO9781107415324.004>
- Marshall, A. G., Hendon, H. H., & Hudson, D. (2016). Visualizing and verifying probabilistic forecasts of the Madden-Julian oscillation. *Geophysical Research Letters*, 43(23), 12278–12286. <https://doi.org/10.1002/2016GL071423>
- Martin, Z., Barnes, E., & Maloney, E. (2021). Predicting the MJO using interpretable machine-learning models (Tech. Rep.). *Atmospheric Sciences*. <https://doi.org/10.1002/essoar.10506356.1>
- Neena, J. M., Lee, J. Y., Waliser, D., Wang, B., & Jiang, X. (2014). Predictability of the Madden-Julian oscillation in the intraseasonal variability hindcast experiment (ISVHE). *Journal of Climate*, 27(12), 4531–4543. <https://doi.org/10.1175/JCLI-D-13-00624.1>
- Palmer, T. N. (2000). Predicting uncertainty in forecasts of weather and climate. *Reports on Progress in Physics*, 63(2), 71–116. <https://doi.org/10.1088/0034-4885/63/2/201>
- Pang, B., Chen, Z., Wen, Z., & Lu, R. (2016). Impacts of two types of El Niño on the MJO during boreal winter. *Advances in Atmospheric Sciences*, 33(8), 979–986. <https://doi.org/10.1007/s00376-016-5272-2>
- Pohl, B., & Matthew, A. J. (2007). Observed changes in the lifetime and amplitude of the Madden-Julian oscillation associated with interannual ENSO sea surface temperature anomalies. *Journal of Climate*, 20(11), 2659–2674. <https://doi.org/10.1175/JCLI4230.1>
- Reichstein, M., Camps-Valls, G., Stevens, B., Jung, M., Denzler, J., Carvalhais, N., & Prabhat (2019). Deep learning and process understanding for data-driven Earth system science. *Nature*, 566(7743), 195–204. <https://doi.org/10.1038/s41586-019-0912-1>
- Roulston, M. S., & Smith, L. A. (2002). Evaluating probabilistic forecasts using information theory. *Monthly Weather Review*, 130(6), 1653–1660. [https://doi.org/10.1175/1520-0493\(2002\)130<1653:EPFUIT>2.0.CO;2](https://doi.org/10.1175/1520-0493(2002)130<1653:EPFUIT>2.0.CO;2)
- Russakovsky, O., Deng, J., Su, H., Krause, J., Satheesh, S., Ma, S., et al. (2015). Imagenet large scale visual recognition challenge. *International Journal of Computer Vision*, 115(3), 211–252. <https://doi.org/10.1007/s11263-015-0816-y>
- Scalia, G., Grambow, C. A., Pernici, B., Li, Y.-P., & Green, W. H. (2019). Evaluating scalable uncertainty estimation methods for DNN-based molecular property prediction.
- Schultz, M., Betancourt, C., Gong, B., Kleinert, F., Langguth, M., Leufen, L., et al. (2021). Can deep learning beat numerical weather prediction? *Philosophical Transactions of the Royal Society A*, 379.
- Slingo, J., & Palmer, T. (2011). Uncertainty in weather and climate prediction. *Philosophical Transactions of the Royal Society A: Mathematical, Physical & Engineering Sciences*, 369(1956), 4751–4767. <https://doi.org/10.1098/rsta.2011.0161>
- Slingo, J. M., Rowell, D. P., Sperber, K. R., & Nortley, F. (1999). On the predictability of the interannual behaviour of the Madden-Julian oscillation and its relationship with El Niño. *Quarterly Journal of the Royal Meteorological Society*, 125(554), 583–609. <https://doi.org/10.1256/smsqj.55410>
- Toms, B. A., Kashinath, K., Yang, D., & Yang, D. (2020). Testing the reliability of interpretable neural networks in geoscience using the Madden-Julian oscillation. *Geoscientific Model Development Discussions*, 1–22. <https://doi.org/10.5194/gmd-2020-152>
- Vitart, F. (2017). Madden-Julian oscillation prediction and teleconnections in the S2S database. *Quarterly Journal of the Royal Meteorological Society*, 143(706), 2210–2220. <https://doi.org/10.1002/qj.3079>
- Vitart, F., Ardilouze, C., Bonet, A., Brookshaw, A., Chen, M., Codorean, C., et al. (2017). The subseasonal to seasonal (S2S) prediction project database. *Bulletin of the American Meteorological Society*, 98(1), 163–173. <https://doi.org/10.1175/bams-d-16-0017.1>. <ftp://s2sidx:s2sidx@acquisition.ecmwf.int/RMMS>
- Vitart, F., & Robertson, A. W. (2018). The sub-seasonal to seasonal prediction project (S2S) and the prediction of extreme events. *Npj Climate and Atmospheric Science*, 1(1), 1–7. <https://doi.org/10.1038/s41612-018-0013-0>
- Wheeler, M. C., & Hendon, H. H. (2004). An all-season real-time multivariate MJO Index: Development of an index for monitoring and prediction. *Monthly Weather Review*, 132(8), 16–1932. [https://doi.org/10.1175/1520-0493\(2004\)132<1917:aarmmi>2.0.co;2](https://doi.org/10.1175/1520-0493(2004)132<1917:aarmmi>2.0.co;2)

- Wu, J., Ren, H. L., Zuo, J., Zhao, C., Chen, L., & Li, Q. (2016). MJO prediction skill, predictability, and teleconnection impacts in the Beijing climate center atmospheric general circulation model. *Dynamics of Atmospheres and Oceans*, *75*, 78–90. <https://doi.org/10.1016/j.dynatmoce.2016.06.001>
- Yoo, C., Lee, S., & Feldstein, S. B. (2012). Arctic response to an MJO-like tropical heating in an idealized GCM. *Journal of the Atmospheric Sciences*, *69*(8), 2379–2393. <https://doi.org/10.1175/jas-d-11-0261.1>
- Zhang, C. (2013). Madden-Julian oscillation: Bridging weather and climate. *Bulletin of the American Meteorological Society*, *94*(12), 1849–1870. <https://doi.org/10.1175/BAMS-D-12-00026.1>

References From the Supporting Information

- Ghiasi, G., Lin, T.-Y., & Le, Q. V. (2018). DropBlock: A regularization method for convolutional networks.
- Hersbach, H. (2000). Decomposition of the continuous ranked probability score for ensemble prediction systems. *Weather and Forecasting*, *15*(5), 559–570. [https://doi.org/10.1175/1520-0434\(2000\)015<0559:DOTCRP>2.0.CO;2](https://doi.org/10.1175/1520-0434(2000)015<0559:DOTCRP>2.0.CO;2)
- Hersbach, H., Bell, B., Berrisford, P., Biavati, G., Horányi, A., Muñoz Sabater, J., et al. (2018a). ERA5 hourly data on pressure levels from 1979 to present. Copernicus climate change service (C3S) climate data store (CDS). <https://doi.org/10.24381/cds.bd0915c6>
- Hersbach, H., Bell, B., Berrisford, P., Biavati, G., Horányi, A., Muñoz Sabater, J., et al. (2018b). ERA5 hourly data on single levels from 1979 to present. Copernicus climate change service (C3S) climate data store (CDS). <https://doi.org/10.24381/cds.adbb2d47>
- Translational Neurotechnology Lab. (2019). *PatternNet GitHub repository*. University of Freiburg. Retrieved from https://github.com/TNTLFreiburg/pytorch_patternnet